Published in final edited form as:
Nat Chem Biol. 2016 December 01; 12(12): 1037–1045. doi:10.1038/nchembio.2193.

Nuclear receptors control pro-viral and antiviral metabolic responses to hepatitis C virus infection

Gahl Levy[#1,2], **Naomi Habib**[#1,2,3], **Maria Angela Guzzardi**[#1,4], **Daniel Kitsberg**[1,2], **David Bomze**[1,2], **Elishai Ezra**[1,5], **Basak E Uygun**[6], **Korkut Uygun**[6], **Martin Trippler**[7], **Joerg F Schlaak**[7], **Oren Shibolet**[8], **Ella H Sklan**[9], **Merav Cohen**[1,2], **Joerg Timm**[10], **Nir Friedman**[1,2], **Yaakov Nahmias**[1,2,*]

[1]Grass Center for Bioengineering, Benin School of Computer Science and Engineering, The Hebrew University of Jerusalem, Jerusalem, Israel

[2]Silberman Institute of Life Sciences, The Hebrew University of Jerusalem, Jerusalem, Israel

[3]Klarman Cell Observatory, Broad Institute of Harvard and MIT, Cambridge, Massachusetts, USA

[4]Institute of Clinical Physiology, National Research Council (CNR), Pisa, Italy

[5]Faculty of Engineering, Jerusalem College of Technology, Jerusalem, Israel

[6]Center for Engineering in Medicine, Massachusetts General Hospital, Boston, Massachusetts, USA

[7]Department of Gastroenterology and Hepatology, University Hospital, University Duisburg-Essen, Essen, Germany

[8]Liver Unit, Department of Gastroenterology, Tel-Aviv Medical Center, Tel Aviv, Israel

[9]Department of Clinical Microbiology and Immunology, Sackler School of Medicine, Tel Aviv University, Tel Aviv, Israel

[10]Institute for Virology, Medical Faculty, University of Düsseldorf, Düsseldorf, Germany

[#] These authors contributed equally to this work.

Abstract

Viruses lack the basic machinery needed to replicate and therefore must hijack the host's metabolism to propagate. Virus-induced metabolic changes have yet to be systematically studied in the context of host transcriptional regulation, and such studies should offer insight into host–pathogen metabolic interplay. In this work we identified hepatitis C virus (HCV)-responsive regulators by coupling system-wide metabolic-flux analysis with targeted perturbation of nuclear

[*]Correspondence and requests for materials should be addressed to Y.N. ynahmias@cs.huji.ac.il.

Author contributions

G.L., N.H., M.A.G., D.K., D.B., J.F.S. and Y.N. designed and performed experiments and analyzed data; E.E., B.E.U., K.U., M.T., O.S., E.H.S., M.C., J.T. and N.F. provided materials, technical support and conceptual advice; Y.N. administered experiments and wrote the paper.

Competing financial interests

The authors declare no competing financial interests.

Europe PMC Funders Author Manuscripts

receptors in primary human hepatocytes. We found HCV-induced upregulation of glycolysis, ketogenesis and drug metabolism, with glycolysis controlled by activation of HNF4α, ketogenesis by PPARα and FXR, and drug metabolism by PXR. Pharmaceutical inhibition of HNF4α reversed HCV-induced glycolysis, blocking viral replication while increasing apoptosis in infected cells showing virus-induced dependence on glycolysis. In contrast, pharmaceutical inhibition of PPARα or FXR reversed HCV-induced ketogenesis but increased viral replication, demonstrating a novel host antiviral response. Our results show that virus-induced changes to a host's metabolism can be detrimental to its life cycle, thus revealing a biologically complex relationship between virus and host.

Viral infection is one of the leading medical challenges of the 21st century. Viruses are parasites that lack the basic metabolic machinery needed to replicate or assemble and therefore must hijack host processes to complete their life cycle. Early research on metabolic changes in infected cells used ^{13}C tracing of glucose and glutamine to show that human cytomegalovirus (HCMV) infection induces glycolysis and fatty acid synthesis in fibroblasts[1]. Direct pharmacological inhibition of this pathway suppresses HCMV replication[2]. More recently, lipidomics has been used to identify fatty acids and lipid mediators critical for influenza replication in A549 cells[3,4]. Again, reversal of virus-suppressed ω3-polyunsaturated fatty acid (PUFA) metabolism was shown to block viral replication[4]. System-wide proteomic and transcriptomic analysis of HCV infection in replicating Huh7.5 cells has suggested that the virus similarly hijacks host metabolism to support its replication, assembly and egress[5,6]. Together, these findings suggest that viruses evolved as metabolic engineers, modulating host processes to optimize virus production.

Our focus was HCV infection, a pandemic affecting 3% of the world's population[7]. This nonintegrating virus replicates in liver cells, causing fatty liver disease and type 2 diabetes[8,9]. The underlying cause of these metabolic changes is difficult to study owing to the lack of biopsy samples from patients in the early stages of infection and difficulties infecting primary hepatocytes in culture[10]. Nevertheless, studies using derivatives of the Huh7 cell line have shown that HCV strongly depends on host lipid metabolism for its replication, assembly and egress[11]. Proteomic analysis of HCV infection in Huh7 cells has shown that, like HCMV and influenza, HCV induces glycolytic enzymes but paradoxically upregulates the enzymes of oxidative phosphorylation as well[6]. Enigmatically, several studies have demonstrated upregulation of both lipid peroxidation and lipid accumulation in infected Huh7 cells[5,6].

Interestingly, host metabolic processes are regulated on the transcriptional level by a network of ligand-activated transcription factors called nuclear receptors[12]. Unraveling the connections between transcriptional regulators and the virus-induced metabolic response would permit systematic modulation of metabolic pathways, enabling scientists to probe the complexity of host–virus interactions. Regretfully, transcriptional control of metabolism is often obscured by other, massive disease-induced transcriptional responses, such as inflammation and wound healing. Consequently, attempts to link metabolic fluxes to transcriptional regulation thus far have been carried out primarily in single-cell organisms[13].

Here we overcame the technical barriers to *in vitro* study of HCV infection by using oxygenated cocultures of primary human hepatocytes that support normal gene expression levels and protein function[14]. We found that these cocultures supported robust HCV infection, which caused metabolic changes that stabilized after 8 d of culture (Fig. 1). This stable experimental system allowed us to use targeted metabolomics to derive a complete metabolic network induced by HCV infection. Using this metabolic network, we identified differentially activated metabolic fluxes and corresponding changes in gene expression. We identified transcriptional regulators, validated them experimentally using a library of GFP reporters, and systematically perturbed their activity using small-molecule inhibitors. Our analysis showed that HCV-infected primary hepatocytes become dependent on an HNF4α-induced shift from oxidative phosphorylation to glycolysis. In addition, we clarify the paradoxical disconnect between lipid oxidation and accumulation, and concomitantly show that drug metabolism was significantly induced by HCV infection in this study. Finally, we confirmed our findings using patient serum and biopsy samples. Our work elucidates the metabolic fingerprint of HCV infection, identifying distinct assemblies of transcriptional–metabolic regulatory circuits in primary human hepatocytes.

Results

Robust HCV infection of primary human hepatocytes

We cocultured freshly isolated primary human hepatocytes with endothelial cells expressing the HCV capture receptor L-SIGN[15]. Cells were seeded in 95% oxygen under serum-free conditions[14] and infected with the JFH-1 cell-culture variant of HCV or a mock-infection control on the first day of culture (Fig. 1a). Hepatocytes cocultured with L-SIGN-expressing endothelial cells showed 2.6-fold higher levels of intracellular HCV RNA after 10 d of infection compared with those cultured alone ($P < 0.05$; Supplementary Results, Supplementary Fig. 1). Primary hepatocyte morphology was markedly altered by HCV infection. Naive cells displayed a cuboidal morphology, smooth cytoplasm and bright cell borders indicative of differentiated, healthy cells. In contrast, JFH-1-infected cells were noticeably smaller and contained numerous lipid droplets in their cytoplasm (Fig. 1b). To visualize infection and lipid accumulation, we infected hepatocytes with a JC1 variant of HCV that contained an in-frame insertion of RFP in the NS5A viral protein[16] (hereinafter called JC1-RFP) and counterstained for intracellular triglycerides (Fig. 1c). Fluorescence microscopy showed that 50% ± 15% of the hepatocytes were positive for HCV after 10 d of infection. HCV production stabilized after 8 d of infection, reaching 30% of the RNA level of model cells (Huh7.5.1 infected with JFH-1) and infectivity titers of 400 focus forming units (f.f.u.) per ml (Fig. 1d). Intracellular analysis showed HCV core protein levels of 6.2 ± 2 fmol per mg protein and a 4.4-fold increase in intracellular triglycerides ($P < 0.05$); these results confirm steatosis, a clinical hallmark of infection (Fig. 1d). Interestingly, although JFH-1-infected Huh7.5.1 cells showed a marked increase in apoptosis upon infection, no significant cell death was observed in primary hepatocytes. Cell viability remained constant above 90% ± 5% with minimal ALT release (Supplementary Fig. 1).

Long-term analysis of metabolic activity showed clear differences between HCV-infected and uninfected cocultures (Fig. 1e, Supplementary Fig. 1). Glucose uptake rates in JFH-1-

infected cocultures were 29% ± 5% higher ($P < 0.01$), whereas urea and albumin production were consistently 39% ± 4% and 70% ± 7% lower ($P < 0.01$), respectively. Lactate and ketone body production were both elevated, whereas the production of triglyceride was dramatically reduced by 69% ± 20% ($P < 0.01$). Similar to previous reports[10], we observed metabolic changes occurring 4 d post-infection, when HCV infectivity began to peak. Metabolic changes stabilized 8 d post-infection, correlating with HCV production reaching a steady state (Fig. 1d,e).

Metabolic fingerprint of HCV infection

The stabilization of primary hepatocyte metabolism, and the quiescent state of the cells, simplifies the derivation of intracellular fluxes by applying mass balance around basic metabolites at pseudosteady state[17] (Supplementary Tables 1 and 2). In total, 31 different metabolites were measured by targeted metabolomics over 48 h on days 9–11 of culture (Online Methods), and the cells were lysed on day 11 for protein and mRNA analysis. Figure 2a shows the metabolic fingerprint of HCV infection, with HCV up- and downregulated metabolic fluxes. Several pathways show clear, statistically significant ($P < 0.05$), coordinated changes after HCV infection. These include the upregulation of glycolysis toward lactate production (flux 1–8) as well as upregulation of ketone body production (flux 47–50). In contrast to previous proteomic studies using Huh7 cells[6], cholesterol and bile acid synthesis were strongly downregulated (flux 76–79), as were glutamine and nitrogen metabolism (flux 15–20) and oxidative phosphorylation (flux 10–14).

To validate our results, we quantified changes in oxidative phosphorylation, fatty acid oxidation and glycolysis in JFH-1-infected primary hepatocytes and in cells treated with sofosbuvir, an antiviral with direct action against HCV[18] (Online Methods). JFH-1 infection caused a 36% ± 4% drop in oxidative phosphorylation, indicating a significant shift to glycolysis ($P < 0.0001$; Fig. 2b,c, Supplementary Figs. 2 and 10). Sofosbuvir treatment reversed this effect, but function remained lower than in naive cells ($P < 0.001$), possibly because of residual HCV or lingering damage (Fig. 2b,c). In contrast, HCV infection increased fatty acid oxidation by 85% ± 29% ($P < 0.02$), and this effect was also reversed by treatment with sofosbuvir ($P = 0.058$; Fig. 2b,c, Supplementary Fig. 2). Finally, HCV infection increased glycolysis by 169% ± 10% ($P < 4 \times 10^{-5}$), and the effect was completely reversed by treatment with sofosbuvir ($P = 0.368$; Fig. 2b,c, Supplementary Fig. 2). This well-coordinated transition from energetic to glycolytic phenotype (known as the Warburg effect) and fatty acid oxidation, coupled with inhibition of the urea cycle, is markedly similar to the metabolic transformation of liver cancer[19].

Regulation of HCV-induced metabolic transformation

Gene expression analysis of naive and HCV-infected primary hepatocytes identified 893 differentially expressed genes (false discovery rate (FDR) q-threshold < 0.05). Unbiased enrichment analysis identified multiple affected processes, including wound healing ($P < 6.3 \times 10^{-12}$), oxidative stress ($P < 3.2 \times 10^{-8}$) and drug and lipid metabolism (Supplementary Fig. 3). Gene-set enrichment analysis (GSEA) focused on metabolic terms showed significant HCV-induced upregulation of drug metabolism ($P < 0.0001$), fatty acid oxidation

($P < 0.0065$) and glycolysis ($P < 0.05$), as well as downregulation of oxidative phosphorylation (Supplementary Fig. 4). Changes in gluconeogenesis and fatty acid biosynthesis were not significant ($P > 0.135$).

These HCV-induced metabolic changes suggest underlying transcriptional regulation. To elucidate this regulation, we grouped functional annotations into six metabolic categories that were sufficiently large for our statistics[20,21] (Supplementary Table 3). The differentially expressed genes were enriched in lipid metabolism ($P < 3.2 \times 10^{-8}$), cholesterol metabolism ($P < 2.4 \times 10^{-12}$), glucose metabolism ($P < 1.2 \times 10^{-14}$) and drug metabolism ($P < 1.1 \times 10^{-13}$). We found 214 differentially expressed genes (24%) involved in metabolic processes (Supplementary Fig. 3). To identify regulators, we searched for transcription factors with target genes that were differentially expressed during HCV infection (Supplementary Tables 4 and 5). Targets were taken from the Biobase database and computationally validated using genome-wide binding data for HNF4α and CEBPα in human hepatocytes[22], as well as mouse overexpression data[23]. Our unbiased search for regulators identified 14 transcription factors controlling the observed changes in metabolic genes, including 12 nuclear receptors known to have a role in regulating the metabolic pathways identified above. We constructed GFP activity reporters for the 14 transcription factors but were able to experimentally validate only seven functional reporters (Supplementary Fig. 5).

HNF4α-induced glycolysis is an HCV proviral response

HCV-infected primary hepatocytes significantly upregulate glycolysis toward the production of lactate ($P < 0.01$) while decreasing mitochondrial oxidative phosphorylation, suggesting a Warburg-like effect in nonproliferating primary hepatocytes (Figs. 2b,c and 3a). GSEA showed significant HCV-induced upregulation of glycolysis but no significant change in gluconeogenesis (Fig. 3a, Supplementary Fig. 4). An unbiased search for transcriptional regulators of glycolysis showed that HCV infection activated HNF1α (MODY3) and HNF4α (MODY1), factors implicated in the development of maturity-onset diabetes of the young (MODY), a hereditary form of diabetes (Fig. 3b,c). The change in expression of regulators and key target genes was independently confirmed by qRT-PCR (Fig. 3d).

To validate the casual role of HNF4α in a rigorous model of HCV infection, we electroporated JC1-RFP or polymerase-negative (Pol^-) HCV RNA into Huh7.5.1 cells (Online Methods). Cells were then infected with an HNF4α activity reporter in which binding of an activated nuclear receptor drives EGFP expression (Fig. 3e). HNF4α activity was greater by a factor of 4 ± 1 in HCV-positive cells compared to Pol^- control (Supplementary Fig. 5). HNF4α activation was reversed after treatment with the HNF4α antagonists Medica16 and BI6015 (refs. 24,25; Fig. 3e). Huh7.5.1 cells replicating JC1-RFP produced more lactate, the end product of glycolysis, than Pol^- controls did ($P < 0.05$). However, treatment with Medica16, BI6015 or short interfering RNA (siRNA) reversed this increase in glycolysis ($P < 0.001$; Fig. 3f, Supplementary Figs. 6 and 7). Importantly, HCV replication was blocked by treatment with either Medica16 ($P = 0.016$) or BI6015 ($P < 0.001$), leading to a three- to fourfold decrease in viral RNA both in cells infected with JC1 (genotype 2a) and in full-length genotype 1b replicon cells[26], as well as in primary human hepatocytes (Fig. 3e,g, Supplementary Figs. 8 and 9).

To confirm that HCV relies on glycolysis, we treated Huh7.5.1 cells replicating JC1-RFP with the glycolytic inhibitors 2DG and BrPA, as well as DCA, a PDK1 inhibitor (Fig. 3h, Supplementary Fig. 13). Treatment with 2DG and BrPA blocked HCV replication ($P < 0.001$), whereas downstream treatment with DCA showed marginal inhibition ($P < 0.05$), demonstrating viral reliance on glycolytic by-products (Fig. 3h). Moreover, HCV infection caused liver cells to become sensitive to Medica16, showing a fourfold increase in apoptosis over Pol$^-$ controls (Fig. 3i,j). These results show a strong proviral effect of HCV-induced glycolysis.

HCV-induced lipid oxidation is an antiviral response

HCV infection has a puzzling effect on lipid metabolism, as cells show both lipid accumulation and oxidation at the same time[5,6]. The involvement of the PPARα transcription factor in this process has been under debate[27,28]. We found that HCV-infected primary hepatocytes significantly upregulated fatty acid oxidation toward the production of ketone bodies ($P < 0.01$) while downregulating cholesterol biosynthesis ($P < 0.01$; Figs. 2b and 4a, Supplementary Fig. 2). Surprisingly, GSEA showed upregulation of both (Supplementary Fig. 4). However, we identified two bifurcation points. First, induction of HMGCL over HMGCR directs acetyl-CoA toward ketone bodies rather than cholesterol (Fig. 4a), and induction of ADRP directs part of the triglyceride flux to lipid droplets rather than lipoproteins (Fig. 4a). An unbiased search for transcriptional regulators of lipid metabolism revealed a hierarchal interconnected network of transcription factors with a role in lipid metabolism (Fig. 4b). The nuclear receptors PPARα, SREBP, FXR and LXRα are known regulators of fatty acid oxidation (PPARα), cholesterol metabolism (SREBP and FXR) and bile acid metabolism (LXRα). Figure 4c shows the links between PPARα, FXR and the metabolic pathway. Regulators and target genes for each factor were independently confirmed by qRT-PCR (Fig. 4d).

We again sought to validate our findings in Huh7.5.1 cells robustly infected with JC1-RFP or Pol$^-$ controls. Cells were infected with PPARα, SREBP, FXR and LXRα activity reporters (Fig. 4b and Supplementary Fig. 5). Although the activity of SREBP and LXRα did not change, we observed a threefold induction of PPARα activity ($P < 0.001$) and a 3.8-fold induction of FXR activity ($P < 0.001$) in HCV-infected cells versus Pol$^-$ controls (Fig. 4e). Activation of PPARα was reversed by treatment with its inhibitors GW9662 and GW6471, and FXR activation was blocked by its inhibitor BML-GR235 (Z-guggulsterone; Fig. 4e,g). Huh7.5.1 cells replicating JC1-RFP showed a two-fold increase in ketone body production and a two-fold decrease in bile acid production, respective end products of fatty acid oxidation and cholesterol biosynthesis (Fig. 4f). Importantly, treatment with GW9662 or GW6471 reversed the HCV-induced increase in ketone body production ($P < 0.001$), and treatment with BML-GR235 reversed the decrease in bile acid production ($P < 0.001$; Fig. 4f). siRNA against each regulator showed similar results (Supplementary Fig. 6). Inhibition by these compounds provides internal controls showing independent PPARα regulation of fatty acid oxidation and FXR regulation of cholesterol biosynthesis (Supplementary Fig. 7). Interestingly, all three inhibitors increased replication of HCV genotype 2a by 40–50%, leading to a 1.4-fold increase in viral RNA (Fig. 4g). A similar 1.8- to 2.4-fold increase in HCV was seen for the genotype 1b replicon in primary human hepatocytes (Supplementary

Figs. 8 and 9). To confirm that HCV relies on fatty acid oxidation, we treated Huh7.5.1 cells replicating JC1-RFP with etomoxir and ranolazine, inhibitors of fatty acid oxidation (Fig. 4h, Supplementary Fig. 13). Treatment with etomoxir and ranolazine increased HCV replication ($P < 0.001$) by 2- and 1.5-fold, respectively.

To probe the second bifurcation point (Fig. 4a), we used intracellular fluorescent staining to quantify lipid accumulation (Online Methods). We found that PPARα inhibition led to increased lipid accumulation (Fig. 4i,j). We note that the HCV life cycle is dependent on lipid accumulation in droplets[29] as well as on cholesterol biosynthesis for FBL2 anchoring[30]. Therefore, in contrast to HNF4α induction of glycolysis, the observed activation of PPARα and FXR during HCV infection is detrimental for the virus life cycle and might be part of a host metabolic antiviral response to infection.

HCV activation of PXR induces hepatic drug metabolism

Changes in hepatic drug metabolism can affect drug clearance rates but are difficult to assess in Huh7.5.1 cells owing to marginal expression of CYP450 enzymes. CYP3A4 is responsible for the clearance of 40% of drugs on the market, including newly introduced antivirals. Our experimental system of primary human hepatocytes does not share this limitation and showed eightfold and sixfold upregulation of CYP3A4 and CYP2C9, respectively, in response to viral infection ($P < 0.001$; Fig. 5c). Other important drug-clearance enzymes such as CYP1A2, 2E1 and 2D6 showed a similar two- to sixfold increase ($P < 0.05$; Supplementary Fig. 11). To confirm these results, we carried out CYP450 activity assays in JFH-1-infected primary human hepatocytes. CYP3A4 and CYP2E1 showed twofold and threefold increases in activity, respectively ($P < 0.05$), confirming our results (Fig. 5e).

An unbiased search for transcriptional regulators of drug metabolism revealed a small network of transcription factors with roles in drug metabolism (Fig. 5a). Figure 5b shows the links among HNF4α, PXR, CAR and the CYP450 enzymes. Regulators and target genes were independently confirmed by qRT-PCR (Fig. 5c). We sought to validate these findings in Huh7.5.1 cells robustly infected with JC1-RFP or Pol^- controls. Cells expressing the PXR activity reporter showed a 5.3-fold induction of PXR activity ($P < 0.05$) in HCV-infected cells compared to Pol^- controls (Fig. 5d, Supplementary Fig. 5). Activation of PXR was reversed by its inhibitor silibinin[31] without observable effects on viral replication (Fig. 5d). Exposure to silibinin blocked the HCV-induced induction of CYP3A4 activity, reversing the effect of PXR (Fig. 5e).

Clinical validation of HCV-induced metabolic changes

Our *in vitro* primary human hepatocyte cocultures reproduced known clinical features of HCV infection predict others (Fig. 1). To test these predictions, we analyzed gene expression in liver biopsy samples obtained from HCV patients in early stages of infection and compared them to healthy controls (Online Methods). Although *in vivo* gene expression levels seldom correlate with *in vitro* levels, expression in primary human hepatocytes was strongly correlated to expression in biopsies of healthy liver, with $R^2 = 0.85$ (Fig. 6a). We identified 1,259 genes that were differentially expressed in liver biopsies during HCV

infection (FDR $q < 0.01$). However, in spite of the well-known metabolic problems associated with HCV infection, unbiased enrichment analysis did not identify any metabolic terms due to overlapping processes such as an immune response ($P < 5.2 \times 10^{-3}$), underscoring the need for *in vitro* analysis.

However, genes differentially expressed *in vivo* were enriched with those found *in vitro* ($P < 0.005$), as well as with genes involved in glucose, lipid and drug metabolism (Supplementary Figs. 3 and 4). Limiting our analysis to metabolic genes, we found that 88% of the genes induced by HCV infection *in vitro* (Fig. 6b) were similarly induced *in vivo*. For example, *CYP450* expression increased with HCV infection both *in vivo* and *in vitro* (Supplementary Fig. 11). However, genes downregulated by HCV infection *in vitro* were randomly distributed in terms of *in vivo* expression (Fig. 6b), possibly because of the presence of multiple cell types (i.e., immune cells) in liver biopsies. An unbiased search for transcriptional regulators *in vivo* revealed a similar network of transcription factors enriched for differentially expressed metabolic genes, including HNF4α, PPARα and FXR (Fig. 6d).

To further test our metabolic findings, we obtained plasma samples from HCV patients in early stages of infection and compared them to samples from healthy control subjects (Fig. 6c). There was marginally more alanine transaminase (ALT) in plasma from HCV patients (97 U/L versus 21 U/L), confirming low levels of inflammation due to steatosis ($P < 0.001$). Serum cholesterol levels were 17% lower ($P < 0.01$) during infection, as has been previously shown[32]. In addition, there was a small (13%) increase in serum glucose levels ($P < 0.05$), suggesting disturbed glycemic control. Importantly, we found that circulating bile acid levels decreased by 53% ($P < 0.05$), whereas levels of β-hydroxybutyrate (βHB) ketone bodies increased by 36% ($P < 0.05$). Lactate levels showed a minor increase of 13%. These results strongly support our *in vitro* observations, confirming the rapid metabolic changes taking hold in early stages of HCV infection.

Discussion

Metabolism is a complex phenomenon regulated on multiple levels. In recent years, a family of ligand-activated transcription factors called nuclear receptors have emerged as key regulators of metabolic processes. Nuclear receptors are activated by metabolites such as fatty acids and glucose, and they control negative feedback loops[12,33], offering an opportunity to reprogram metabolism at the transcriptional level. This approach is appealing in the context of metabolic disease and viral infection, where pharmaceutical targeting of transcriptional regulators could rewire chronic metabolic states.

In this work, we studied the effects of HCV infection on primary human hepatocytes. Our cocultures of primary human hepatocytes with L-SIGN$^+$ endothelial cells showed robust infection, affecting 50% of the cells (Fig. 1), compared with previously reported infection rates of 6–10% (ref. 10). Similar infection rates, ranging from 20% to 50%, have been found *in vivo*[34,35]. In contrast to earlier work on Huh7 cells, infection of primary hepatocytes reproduced lipid accumulation and hypolipidemia, clinical hallmarks of infection, matching the transcriptional and metabolic signature of patient samples (Fig. 6). This allowed us to

track metabolic changes with confidence and correlate these changes to their underlying transcriptional regulators (Figs. 3–5).

The effect of HCV infection on CYP450 expression is an area of major interest for pharmaceutical development, and it could not be studied in Huh7 cells, as tumors show minimal expression of CYP450 enzymes. We show that HCV upregulates CYP3A4 both *in vitro* and *in vivo* (Fig. 5). This increase would affect the clearance rates of emerging antiviral drugs that are substrates of CYP3A4, such as telaprevir, boceprevir and simeprevir.

We also show that HCV infection of primary hepatocytes induces glycolysis over oxidative phosphorylation in a manner similar to HCMV infection of fibroblasts[2] and the Warburg effect in cancer[36,37]. Although upregulation of glycolysis has been previously observed in HCV-infected Huh7.5 cells via proteomic analysis[6], so have oxidative phosphorylation and glutamine metabolism[6]. This suggests that the global upregulation of metabolic pathways previously reported was a result of HCV-induced upregulation of Huh7.5 proliferation, rather than the host response to infection[38]. In contrast, our model shows a striking induction of glycolysis over oxidative phosphorylation in both primary human hepatocytes and growth-arrested Huh7.5 cells (Supplementary Fig. 10), strengthening earlier evidence of HCMV-induced glycolysis in serum-starved fibroblasts[2].

An unbiased search for metabolic regulators showed that HNF4α, a nuclear receptor associated with MODY[39], has a critical role in host glycolytic response. Although there are conflicting reports regarding HNFs in HCV infection[40,41], our work clearly shows that HNF4α inhibition reverses glycolysis in infected cells. Suppression of glycolysis by Medica16, BI6015 or the glycolytic inhibitors 2DG and BrPA blocked HCV replication as a result of substrate limitation (Fig. 3). Importantly, the treatment also increased apoptosis in HCV-infected cells, suggesting that the process is driven by host reliance on nonoxidative energy (Fig. 2) rather than by the needs of the virus.

Unraveling lipid metabolism proved more complex. Early analysis of HCV-infected Huh7 cells suggested cross-purpose induction of both fatty acid oxidation and lipogenesis[6]. Lipogenesis is similarly induced in HCMV infection and certain types of cancer[42], but not in HCV infection of primary hepatocytes. In fact, lipid peroxidation has recently been shown to attenuate HCV replication and egress[43,44]. Our results show PPARα-dependent induction of fatty acid oxidation and FXR-dependent suppression of cholesterol biosynthesis (Fig. 4). Similar activation of FXR has a critical role in liver carcinogenesis[45]. These results are surprising, as HCV relies on cholesterol biosynthesis to anchor its NS5A cofactor through FBL2 (ref. 46) and on lipid droplets for replication and lipoprotein-dependent egress[29,47]. Importantly, inhibition of either nuclear receptor, or of fatty acid oxidation directly, caused considerable upregulation of HCV replication, suggesting that in contrast to HNF4α, the effects of PPARα and FXR are part of a host antiviral response.

In summary, our work provides a metabolic fingerprint of HCV infection in primary human hepatocytes, mapping it to transcriptional regulators that can be pharmaceutically modulated. We show that viral infection dramatically effects host metabolism, but not always for the benefit of the virus. The results show that virus needs can conflict with the

host's requirement for energy and that virus replication might be tightly controlled by positive and negative interactions with the host[48].

Online Methods

Hepatocyte oxygenated cocultures

Primary human hepatocytes were obtained from BD Biosciences or were kindly provided by Dr. Stephen C. Strom (University of Pittsburgh). Human cells were purified in 33% Percoll solution centrifuged at 500*g* for 5 min before seeding. Cell viability post-purification was greater than 90%, and purity was greater than 95%. After purification hepatocytes were mixed with lung endothelial cells (Lonza) at a 4:3 ratio in ice-cold culture medium and seeded at 175,000 cells/cm^2 in a humidified incubator set at 37 °C and conditioned by a gas mixture of 95% oxygen and 5% CO_2 (Airgas). After overnight seeding under 95% oxygen, the cultures were returned to atmospheric levels of oxygen and 5% CO_2. HCV infection was carried out 24 h after seeding (day 1). Cells were cultured in serum-free basal medium (Lonza) supplemented with ascorbic acid, transferrin, EGF and antibiotics. Medium was further supplemented with 100 μg/mL of rat-tail collagen during seeding to enhance attachment[14]. Hepatocyte culture medium was collected every 48 h and stored at −80 °C for metabolic analysis. After 11 d of culture (10 d post-infection) endothelial cells were removed by trypsinization and the hepatocyte population was scraped off the surface for protein and mRNA analysis. Hepatocyte purity post-trypsinization was assessed by immunofluorescence microscopy and was found to be greater than 95%. Cultures were confirmed to be free of mycoplasma contamination using a PCR test kit (Biological Industries).

Drugs and reagents

2-DG (sc-202010), BrPA (sc-296029), and DCA (sc-260854) were purchased from Santa Cruz Biotechnology. GW9662 (M6191), GW6471 (G5045), etomoxir (E1905), ranolazine (R6152), silibinin (S0417), and Medica16 (M5693) were purchased from Sigma-Aldrich. BI6016 (4641) was purchased from Tocris, and BML-GR235 (39025) was purchased from Enzo. A Human Albumin Elisa Quantitation Set (E80-129) was purchased from Bethyl Laboratories. A Human α-Fetoprotein ELISA kit (ab108838) was purchased from Abcam.

JFH-1, JC1-RFP, and polymerase-negative (Pol$^-$) RNA production and electroporation

The Huh7.5.1 human hepatoma cell line was provided by F. Chisari (Scripps Research Institute). Huh7.5.1 cells were cultured in DMEM supplemented with 10% FBS and 200 units/mL penicillin–streptomycin in a 5% CO_2-humidified incubator at 37 °C. Plasmids containing the JFH-1 and JC1-RFP full-length genome were kindly provided by T. Wakita (National Institute of Infectious Diseases) and R. Bartenschlager (University of Heidelberg), respectively. The JFH replicon containing the GND inactivating mutation in the viral polymerase (Pol$^-$) served as negative control. *In vitro* transcribed JFH-1, JC1-RFP and Pol$^-$ RNA were delivered to cells by electroporation using a BTX model 830 electroporator (820 V, five 99-μs pulses given at 220-ms intervals). Cells were left to recover for 15 min at 22 °C and then mixed with 10 mL of pre-warmed growth medium and seeded for further analysis. Fluorescence microscopy showed robust JC1-RFP infection affecting over 90% of the

Europe PMC Funders Author Manuscripts

Huh7.5.1 cells. To generate JFH-1 and JC1-RFP viruses for infection, we collected Huh7.5.1 conditioned medium for 72 h after electroporation. Conditioned medium was concentrated and used to infect primary human hepatocytes at multiplicity of infection of 0.5–1 for 24 h. Culture medium was subsequently changed daily. The mock control consisted of similarly processed medium conditioned by naive Huh7.5.1 cells.

Quantitative reverse-transcription polymerase chain reaction (qRT-PCR)

Virus samples were purified using a QIAamp viral RNA mini kit (Qiagen). The reverse-transcription reaction step was performed on a Mastercycler ep Gradient S (Eppendorf) instrument using a High Capacity cDNA reverse transcription kit (Applied Biosystems). Real-time PCR was performed on a MyiQ real-time PCR detection system using the iScript One-Step RT-PCR kit with SYBR Green (Bio-Rad) according to the respective manufacturers' instructions.

Small-molecule inhibition of nuclear receptor and metabolic targets

JC1-RFP or Pol$^-$ electroporated Huh7.5.1 cells were grown to 90% confluence and treated with small-molecule inhibitors or DMSO control for 24 h. Primary human hepatocytes were similarly treated 10 d post-infection. Cell viability was >90% for all concentrations tested (Supplementary Fig. 12).

Central glycolysis inhibitors 2-deoxy-D-glucose (2DG) and 3-bromopyruvate acid (BrPA) were used at 1 mM and 10 μM, respectively. Dichloroacetate (DCA), which blocks PDK1, redirecting pyruvate to oxidative phosphorylation, was used at 100 μM (ref. 49). Fatty-acid-oxidation inhibitors etomoxir[50] and ranolazine[51] were used at 100 μM and 50 μM, respectively.

The specificity of nuclear-receptor antagonists was validated using qRT-PCR (Supplementary Fig. 5). HNF4α activation was reversed after treatment with 250 μM Medica16 or 5 μM BI6015 (refs. 24,25). PPARα activation was reversed by treatment with 10 μM GW9662 or 10 μM GW6471. FXR was blocked by treatment with 100 μM BML-GR235 (ref. 52), and PXR was blocked by treatment with 200 μM silibinin[31]. HCV levels were determined by qRT-PCR and fluorescence quantification of JC1-RFP normalized to the number of Hoechst-positive nuclei.

HCV infectivity

The production of infectious JFH-1 virus particles by primary hepatocytes was measured as previously described[44]. Briefly, naive Huh7.5.1 cells were grown to 80% confluence and exposed to cell culture supernatants serially diluted tenfold in the culture medium. After overnight incubation at 37 °C, 5% CO_2, the medium was replaced, and cells were cultured for an additional 3 d. Levels of HCV infection were determined by immunofluorescence staining for HCV core protein[47]. The viral titer is expressed in focus forming units (f.f.u.) per milliliter of supernatant.

Biochemical assays

Albumin concentration was determined with a commercial ELISA kit (Bethyl Laboratories). Urea concentration was measured with a blood urea nitrogen kit (Stanbio Labs). Glucose and lactate levels were determined using commercial kits testing for glucose oxidase (Stanbio Labs) and lactate oxidase (Trinity Biotech, Bray), respectively. Triglycerides were quantified using a commercial kit (Sigma Chemical) based on glycerol quantification. Free fatty acids were determined on the basis of their CoA derivatives using a commercial kit (BioVision). The ketone bodies acetoacetate and β-hydroxybutyrate were measured by the disappearance of NADH in the conversion of acetoacetate to β-hydroxybutyrate in the presence of β-hydroxybutyrate dehydrogenase and by the production of NADH in the reverse reaction. Cholesterol was measured using a commercial kit (Stanbio Labs) based on cholesterol oxidase. Total bile acids were determined through NADH formation using a commercial kit (BioQuant). Individual amino acid concentrations in medium samples were quantified by HPLC as previously described[53]. ALT and AST levels were quantified using a commercially available kit (Thermo Fisher Scientific). HCV core proteins were measured using the ORTHO HCV antigen ELISA kit (Ortho Clinical Diagnostics). The oxygen uptake rate was measured in parallel cultures using the Ocean Optics FOXY fiber optic oxygen sensor immersed in a well-stirred chamber as previously described[54].

Metabolic flux balance analysis (MFA)

MFA is a stoichiometric model of hepatocyte metabolism in which intracellular fluxes are calculated via the application of mass balances around basic metabolites. The analytical predictions of the model used in this work were previously confirmed using radiolabeled substrates[55]. The stabilization of primary hepatocyte metabolism 8 d after infection, and the lack of cell proliferation, allowed us to use the model under steady-state conditions, which reduced the balance equations to a set of linear algebraic equations given by $dz/dt = S \times v = 0$, where z represents metabolites, S is an $n \times m$ matrix of coefficients, and v is a vector of m fluxes[17,56]. This approach accounts for the complex interdependence between pathways due to a common pool of cofactors and thus provides a comprehensive picture of the hepatic metabolic state[17,56]. Here we expanded the model to include lipid metabolism, adding fluxes for cholesterol synthesis, bile production, triglyceride synthesis and accumulation. The mathematical model uses 35 metabolites and 80 chemical reactions implemented and solved using MATLAB. Because of linear dependence the matrix is completely determined.

Metabolic flux quantification of HCV-infected and sofosbuvir-treated cells

Primary human hepatocytes were infected with JFH-1 containing medium for 7 d and treated with 10 μM sofosbuvir (Cayman Chemical) or DMSO vehicle control for 72 h. 3.5×10^3 cells were plated on collagen-coated XFp Flux Analyzer Miniplates (Seahorse Bioscience). A mitochondrial stress test assay was conducted per the manufacturer's instructions. Briefly, cells were incubated in unbuffered DMEM supplemented with 2 mM glutamine, 1 mM sodium pyruvate, and 10 mM glucose (pH 7.4) for 1 h at 37 °C in a non-CO_2 incubator. We measured the basal oxygen consumption rate (OCR) for 30 min and then injected 1 μM oligomycin, a mitochondrial complex V inhibitor that blocks oxidative phosphorylation. The decrease in OCR due to oligomycin treatment was defined as the oxidative phosphorylation

rate. 1 μM carbonyl cyanide 4-(trifluoromethoxy)phenylhydrazone (FCCP), an uncoupling agent, was added at 60 min to measure maximal mitochondrial activity, and complete inhibition was induced at 90 min using a mixture of 0.5 μM antimycin A and rotenone, mitochondrial complex III and mitochondrial complex I inhibitors.

Free fatty acid oxidation was measured as previously described[57]. Briefly, after overnight incubation in substrate-limited medium containing 0.5 mM glucose to prime cells for exogenous fatty acid utilization, cells were incubated in unbuffered DMEM supplemented as described above. Basal OCR was measured for 30 min, and then 200 μM palmitate (C16:0) was injected. Fatty acid oxidation was blocked at 60 min by injection of 100 μM etomoxir, a carnitine palmitoyltransferase I (CPT1) inhibitor. OCR attributable to exogenous fatty acid oxidation was defined as the difference between maximal palmitate-treated and minimal etomoxir-treated conditions.

A glycolysis stress test assay was conducted per the manufacturer's instructions. Briefly, cells were incubated in unbuffered DMEM supplemented with 2 mM glutamine and 1 mM sodium pyruvate (pH 7.4) for 1 h at 37 °C in a non-CO_2 incubator. The extracellular acidification rate (ECAR) was measured for 30 min in the absence of glucose; this served as the baseline measurement. We measured the rate of glycolysis by injecting 10 mM glucose at 30 min, followed by 1 μM oligomycin, blocking oxidative phosphorylation at 60 min. Finally, 100 mM 2DG, a nonmetabolized glucose analog, was injected at 90 min to competitively inhibit glycolysis. The increase in ECAR due to the addition of glucose was defined as the glycolysis rate, and the difference between oligomycin and 2DG treatments defined the maximal glycolytic capacity of the cells. Data are presented normalized to 10^4 cells.

Metabolic phenotype comparison was conducted per the manufacturer's instructions, as previously described (ref. 58). Briefly, absolute basal OCR and ECAR levels, normalized to protein concentration, were graphically plotted for naive, JFH-1-infected and sofosbuvir-treated primary human hepatocytes. The graphical representation indicates a relative metabolic phenotype between the three groups, the relative reliance on glycolysis or oxidative phosphorylation.

Generation of transcription factor activity reporter library

We generated transcription factor activity reporters by cloning DNA response elements (i.e., PPRE and LXRE) upstream of a minimal CMV promoter. Binding of an activated transcription factor to its DNA response element induces the transcription of destabilized copGFP with a half-life of 2 h, permitting the measurement of both transcriptional activation and inhibition. Reporters were generated for 14 computationally identified transcription factors including HNF4α, PPARα, FXR, SREBP, LXRα, PPARγ and PXR. To validate their activity, we introduced reporters to Huh7.5.1 or HepG2 cells and stimulated them with a classical agonist (Supplementary Fig. 5).

SREBP1c, LXRα, and PPARγ pGreenFire1 activity reporters were purchased from System Biosciences and validated in-house. Reporters contained ATCACGTG, GGGTTACTGGCGGTCATTGTA and TGTAGGTCACGGTGACCTAC, respectively,

upstream of a minimal CMV promoter. The FXR reporter was constructed by PCR amplification of human genomic DNA from −145 to +86 of the BSEP promoter and subsequent cloning upstream of copGFP. The promoter of BSEP contains an FXR response element (GGGACATTGATCCT). The PPARα reporter was constructed by PCR amplification of human genomic DNA from −562 to +1,890 of the human CPT1A gene and cloning upstream of copGFP. The PXR reporter construct was cloned from the human CYP3A4 promoter and was a kind gift from Dr. C. Liddle (University of Sydney, Australia). The promoter from the original luciferase construct was subcloned into the copGFP construct. We constructed the HNF4 reporter by cloning three HNF4 response elements (GGGTCAAAGGTCA) upstream of the minimal CMV promoter in the same pGreenFire1 reporter construct.

Reporter activity screen in infected Huh7.5.1 cells

Huh7.5.1 cells electroporated with JC1-RFP or Pol$^-$ RNA were re-plated in a black 96-well plate at a density of 5×10^4 cells per well 24 h after electroporation. GreenFire lentivirus reporters were generated according to the manufacturer's directions. Briefly, 293T cells were cotransfected with a pGreenFire1 activity reporter plasmid, a plasmid expressing GAG-Pol, and a plasmid expressing VSV-G in a ratio of 3:2:1. 24 μg of total DNA was diluted in 750 μL of OptiMEM and 25 μL of polyethylenimine, mixed, allowed to settle for 5 min and added to 293T packaging cells cultured without antibiotics. Lentivirus was collected from the supernatant on the third day of culture, filtered through a 45-μm syringe filter, mixed with 4 ng/mL polybrene, and added at 100 μL/well to Huh7.5.1 cells expressing JC1-RFP or Pol$^-$ RNA. Lentivirus infection was repeated the following day and reached >80% efficiency based on the EGFP control.

24 h after the second infection (72 h after electroporation) the cells were imaged using Carl Zeiss LSM700 confocal microscope. Photos were analyzed using ImageJ software. Activity is presented as the number of GFP-positive cells above a preset threshold normalized to the Pol$^-$ control. We quantified HCV replication in the same samples by defining a low threshold, identifying HCV-positive cells, and measuring RFP fluorescence in HCV-positive cells divided by the area of the cells. A minimum of four regions were quantified for each experimental condition.

Intracellular lipid accumulation

Intracellular lipid accumulation was quantified using Nile Red staining (Sigma Chemical) according to the manufacturer's instructions. Briefly, cultures were fixed with 4% formaldehyde in PBS for 20 min at room temperature, washed, treated with 1 μM Nile Red and counterstained with Hoechst 33258 (Sigma Chemical). Images were taken using a Carl Zeiss LSM700 confocal microscope and analyzed using ImageJ software. Lipid accumulation is presented as lipid intensity normalized to Hoechst. A minimum of four regions were quantified for each experimental condition.

Quantification of apoptosis

Quantitation of apoptotic cell nuclei was carried out with the DeadEnd Fluorometric TUNEL assay (Promega) according to the manufacturer's instructions. Briefly, cultures were

fixed with 4% formaldehyde in PBS for 20 min at 4 °C, washed, and permeabilized with 0.2% Triton X100 for 5 min. Cultures were then equilibrated to room temperature for 10 min in buffer and treated with TdT reaction mixture for 60 min at 37 °C. The reaction was stopped using SSC for 15 min, at which point cells were washed and counterstained with Hoechst. Images were taken using aCarl Zeiss LSM700 confocal microscope and analyzed using ImageJ software. Apoptosis is presented as TUNEL intensity normalized to Hoechst. A minimum of four regions were quantified for each experimental condition.

Clinical HCV sample collection

Plasma and liver biopsy samples were obtained from individuals infected with HCV attending the Department of Gastroenterology and Hepatology of the University Hospital Duisburg-Essen, Germany, after obtaining written informed consent. The study was approved by the Institutional Review Board of the University of Essen, Germany (IRB 08-3662). Inclusion criteria included a diagnosis of early HCV infection, defined as HCV RNA abundance greater than 100,000 IU/mL, but fibrosis stage 1 determined using FibroScan or pathological assessment. Patients with HIV or HBV coinfection, decompensated liver disease, or organ transplantation were excluded, as were those on medications that alter lipid metabolism.

Patient plasma samples

Plasma samples were collected from 15 people positive for HCV infection (genotypes 1A, 1B and 3A), after an overnight fast. Patient age ranged from 33 to 72 years; their ALT levels were below 190 U/l, and their fasting glucose levels were below 130 mg/dL. FibroScan results showed only minimal fibrosis.

Patient biopsy samples

Liver biopsy samples were collected from five patients, at early stages of HCV infection (genotypes 2B, 1A, 2A and 3A), after an overnight fast. Patient age ranged from 25 to 39 years, and their GPT levels were below 112 U/l. FibroScan and histological assessment showed minimal fibrosis and low-grade inflammation in the liver samples. Normal human liver biopsy data from 19 patients were taken from GEO accession GSE14323 (ref. 58). The age for these subjects ranged from 9 to 66 years, and their cause of death was primarily head trauma.

Affymetrix gene arrays

In vitro RNA samples were tested on the Affymetrix GeneChip Human Exon 1.0 ST array at the Center for Genomic Technologies at the Hebrew University of Jerusalem. *In vivo* RNA samples were isolated from snap-frozen liver biopsy samples and tested on Affymetrix GeneChip Human Genome U133A 2.0 array at the Genomic Facility of the University Hospital Essen, Germany. Both processes were carried out in an Affymetrix accredited facility according to the company instructions. GSE14323 samples deposited[58] were similarly collected and hybridized to the same Human Genome U133A 2.0 array. Microarray data were deposited in GEO (GSE84587).

Gene expression analysis

After a robust multi-array average (RMA) procedure and quantile normalization, the probes were filtered using BioDiscovery's Nexus Expression software. Probes with a variance less than 0.2 and intensity less than 4.0 were removed. Differential expression of HCV-infected versus naive cells *in vitro* was evaluated via two-sample Student's *t*-test, using a threshold of $P < 0.05$ after Bonferoni correction for multiple hypotheses. Under these conditions, 893 genes were differentially regulated *in vitro*. Patient-to-patient differences required a more stringent test for the *in vivo* samples in order to reduce variability. We therefore carried out a two-sample Student's *t*-test using a threshold of $P < 0.01$ after Bonferoni correction for multiple hypotheses and 1.5-fold change. Under these conditions, a similar-sized group of 1,259 genes were found to be differentially regulated *in vivo*.

Assembly of metabolic categories

We defined metabolic categories by uniting various functional annotations chosen by hand, taken from GO[20] or KEGG[21] (Supplementary Table 3). We assembled five sets for metabolic categories and a set of oxidative stress response genes. General liver metabolism was defined as the combination of all metabolic categories.

Functional annotations of gene expression

To functionally annotate differentially expressed genes, we tested for their enrichment in functional gene sets. The general test for functional enrichment of the differentially expressed genes against various functional categories was done using the DAVID tool[59]. We tested the enrichment of differentially expressed genes with metabolic categories (defined above), using all genes expressed *in vitro* as the background list. Enrichment *P* values were calculated using Fisher's exact test and with Bonferoni correction for multiple hypotheses. The analysis of the *in vivo* and *in vitro* data was done the same way, including only genes measured on both arrays.

Target genes of transcription factors

Transcription factor target genes were defined by BioBase on the basis of expression analysis and binding data. We added *CAR* as a target gene of HNF4α on the basis of literature reports[60]. We found target genes in the liver for the factors HNF4α and CEBPα for validation using DNA binding data measured by ChIP-seq in primary human hepatocytes[22]. To determine target genes for these two factors, we used the bindingsite locations previously determined[22] and defined a gene as a target of the factor if we found a binding site 3,000 bp upstream or of the transcription start site (TSS) of the gene. TSS locations were downloaded from the human genome version HG19 in the UCSC Genome Browser. We found target genes in the liver for the factors SREBF1, SREBF2 and their negative regulator SCAP using their defined target genes based on overexpression in mouse primary hepatocytes[23]. We mapped the mouse target genes to their human orthologs using orthologous mapping from the MGI database (Informatics).

Transcriptional activity analysis

We conducted an unbiased search for transcription factors differentially regulating metabolic pathways after HCV infection (Supplementary Table 4). A transcription factor was considered to be differentially regulating a pathway if its target genes were enriched with differentially expressed genes within this pathway. Enrichment *P* values were calculated using Fisher's exact test and corrected for multiple hypotheses using a false discovery rate (FDR) threshold of 1%. The analysis was done separately for each constraint metabolic pathway defined above (Supplementary Table 4). We created the full regulatory network of each metabolic pathway in a similar way, but using all genes in each metabolic category.

Similarly, we searched for transcription factors regulating differentially expressed metabolic genes in response to HCV infection by testing the enrichment (FDR threshold of 5%) of transcription factor target genes with differentially expressed metabolic genes *in vitro* (total of 235 genes). To compare the *in vivo* and *in vitro* data, we tested each *in vitro* enriched factor for enrichment (FDR threshold of 5%) of its target genes with the set of metabolic genes differentially expressed *in vivo* (total of 189 genes; Supplementary Table 5).

HCV pseudoparticles (HCVpp)

HCVpp were created by binding of HCV surface receptors E1–E2 to 100-nm-diameter fluorescent beads. Green-fluorescent beads were purchased from Polysciences, Inc. Properly folded E1–E2 heterodimers were recombinantly expressed and linked to beads as previously described[47].

Full-length genotype 1 replicon cells

Huh7 clonal cells harboring a full-length genotype 1b replicon were cultured in DMEM supplemented with 10% FBS and 250 μg/ml G418 in a 5% CO_2–humidified incubator at 37 °C. Cells were grown to 90% confluence and exposed to 250 μM Medica16, 5 μM GW-9662, 10 μM GW-6471, 100 μM BML-GR235, or 0.5% DMSO vehicle control for 24 h. RNA was isolated and purified using a Macherey-Nagel NucleoSpin RNA II kit according to the manufacturer's instructions. RNA concentration and purity were determined using a NanoDrop ND-1000 spectrophotometer (Thermo Fisher Scientific). Gene expression analysis was carried out using a Bio-Rad iScript One-Step RT-PCR kit on the Bio-Rad CFX96 Real-Time system. HCV (forward, 5′-AGAGCCATAGTGGTCTGCGGAA-3′; reverse, 5′-AAATCTCCAGGCATTGAGCGGGTT-3′) gene transcription was evaluated using the $\Delta\Delta C_t$ method normalized to RPL32.

LIVE/DEAD quantification of cell viability

Huh7.5.1 cells and primary human hepatocytes cocultured with endothelial cells were stained using a fluorescent LIVE/DEAD viability assay (Invitrogen Life Sciences) in which the cytoplasm of live cells accumulates green-fluorescent calcein because of esterase activity, while the nuclei of dead cells are labeled red by ethidium homodimer owing to a loss of nuclear membrane integrity. Cells were quantified using ImageJ.

AFP secretion ELISA analysis

Control (Pol$^-$) and JC1-infected Huh7.5.1 cells were treated with Medica16 and BI6015 for 24 h. Supernatant and cell lysate samples were collected. AFP concentration was analyzed using the AFP human ELISA kit (Abcam) according to the manufacturer's directions. All data were normalized to total protein content using the Bradford assay.

Small interfering RNA analysis In Huh7.5.1 cells

Cells were plated in 12-well plates 24 h before transfection at 30–50% confluency. Transfection experiments were performed using Lipofectamine 2000 (Invitrogen). 50 μL solution of siRNAs and LF2K were prepared in Opti-Mem and allowed to mix for 30 min before their addition to cells at final concentrations of 5–100 nM siRNA and 2.3 μg/mL LF2K. Cells were incubated in the transfection solutions at 37 °C and 5% CO_2. After 24 h, cells were washed twice with DPBS (Gibco), and EGFP fluorescence was quantified using a plate reader at 480 nm excitation/525 nm emission. Fluorescence intensity was normalized to control wells that were treated with transfection reagent but no siRNA. Cytotoxicity was assessed by LIVE/DEAD staining.

Statistical analysis

Experiments were repeated two or three times with triplicate samples for each experimental condition. Data from representative experiments are presented, and similar trends were seen in multiple trials. Unless otherwise noted, a parametric two-tailed Student's *t*-test was used to calculate significant differences between groups.

Supplementary Material

Refer to Web version on PubMed Central for supplementary material.

Acknowledgments

The authors thank M.-L. Izamis and M. Zimerman for technical support, K.J. Archer for providing GSE14323 phenotypic data, A. Regev for important insight, and the generous gift of S. Frankel and R. Frankel. Some primary human hepatocytes were kindly provided by S.C. Strom (University of Pittsburgh, Pittsburg, Pennsylvania, USA). The Huh7.5.1 human hepatoma cell line was provided by F. Chisari (Scripps Research Institute, La Jolla, California, USA). Plasmids containing the JFH-1 full-length genome were kindly provided by T. Wakita (National Institute of Infectious Diseases, Tokyo, Japan); plasmids containing the JC1-RFP full-length genome were kindly provided by R. Bartenschlager (University of Heidelberg, Heidelberg, Germany). The PXR reporter construct was a kind gift from C. Liddle (University of Sydney, Australia). This work was funded by European Research Council Starting Grant TMIHCV (project 242699), European Research Council Consolidator Grant OCLD (project 681870) and the British Council BIRAX Regenerative Medicine award (project 06BX14SFYN).

References

1. Munger J, Bajad SU, Coller HA, Shenk T, Rabinowitz JD. Dynamics of the cellular metabolome during human cytomegalovirus infection. PLoS Pathog. 2006; 2:e132. [PubMed: 17173481]
2. Munger J, et al. Systems-level metabolic flux profiling identifies fatty acid synthesis as a target for antiviral therapy. Nat Biotechnol. 2008; 26:1179–1186. [PubMed: 18820684]
3. Tam VC, et al. Lipidomic profiling of influenza infection identifies mediators that induce and resolve inflammation. Cell. 2013; 154:213–227. [PubMed: 23827684]
4. Morita M, et al. The lipid mediator protectin D1 inhibits influenza virus replication and improves severe influenza. Cell. 2013; 153:112–125. [PubMed: 23477864]

5. Woodhouse SD, et al. Transcriptome sequencing, microarray, and proteomic analyses reveal cellular and metabolic impact of hepatitis C virus infection in vitro. Hepatology. 2010; 52:443–453. [PubMed: 20683944]
6. Diamond DL, et al. Temporal proteome and lipidome profiles reveal hepatitis C virus-associated reprogramming of hepatocellular metabolism and bioenergetics. PLoS Pathog. 2010; 6:e1000719. [PubMed: 20062526]
7. Guidotti LG, Chisari FV. Immunobiology and pathogenesis of viral hepatitis. Annu Rev Pathol. 2006; 1:23–61. [PubMed: 18039107]
8. Mihm S. Hepatitis C virus, diabetes and steatosis: clinical evidence in favor of a linkage and role of genotypes. Dig Dis. 2010; 28:280–284. [PubMed: 20460924]
9. Arrese M, Riquelme A, Soza A. Insulin resistance, hepatic steatosis and hepatitis C: a complex relationship with relevant clinical implications. Ann Hepatol. 2010; 9:112–118.
10. Ploss A, et al. Persistent hepatitis C virus infection in microscale primary human hepatocyte cultures. Proc Natl Acad Sci USA. 2010; 107:3141–3145. [PubMed: 20133632]
11. Ikeda M, Kato N. Modulation of host metabolism as a target of new antivirals. Adv Drug Deliv Rev. 2007; 59:1277–1289. [PubMed: 17897752]
12. Chawla A, Repa JJ, Evans RM, Mangelsdorf DJ. Nuclear receptors and lipid physiology: opening the X-files. Science. 2001; 294:1866–1870. [PubMed: 11729302]
13. Moxley JF, et al. Linking high-resolution metabolic flux phenotypes and transcriptional regulation in yeast modulated by the global regulator Gcn4p. Proc Natl Acad Sci USA. 2009; 106:6477–6482. [PubMed: 19346491]
14. Kidambi S, et al. Oxygen-mediated enhancement of primary hepatocyte metabolism, functional polarization, gene expression, and drug clearance. Proc Natl Acad Sci USA. 2009; 106:15714–15719. [PubMed: 19720996]
15. Gardner JP, et al. L-SIGN (CD 209L) is a liver-specific capture receptor for hepatitis C virus. Proc Natl Acad Sci USA. 2003; 100:4498–4503. [PubMed: 12676990]
16. Schaller T, et al. Analysis of hepatitis C virus superinfection exclusion by using novel fluorochrome gene-tagged viral genomes. J Virol. 2007; 81:4591–4603. [PubMed: 17301154]
17. Chan C, Berthiaume F, Lee K, Yarmush ML. Metabolic flux analysis of cultured hepatocytes exposed to plasma. Biotechnol Bioeng. 2003; 81:33–49. [PubMed: 12432579]
18. Murakami E, et al. Mechanism of activation of PSI-7851 and its diastereoisomer PSI-7977. J Biol Chem. 2010; 285:34337–34347. [PubMed: 20801890]
19. Liu L, et al. Deregulated MYC expression induces dependence upon AMPK-related kinase 5. Nature. 2012; 483:608–612. [PubMed: 22460906]
20. Ashburner M, et al. Gene ontology: tool for the unification of biology. Nat Genet. 2000; 25:25–29. [PubMed: 10802651]
21. Kanehisa M, Goto S. KEGG: Kyoto encyclopedia of genes and genomes. Nucleic Acids Res. 2000; 28:27–30. [PubMed: 10592173]
22. Schmidt D, et al. Five-vertebrate ChIP-seq reveals the evolutionary dynamics of transcription factor binding. Science. 2010; 328:1036–1040. [PubMed: 20378774]
23. Horton JD, et al. Combined analysis of oligonucleotide microarray data from transgenic and knockout mice identifies direct SREBP target genes. Proc Natl Acad Sci USA. 2003; 100:12027–12032. [PubMed: 14512514]
24. Kiselyuk A, et al. HNF4α antagonists discovered by a high-throughput screen for modulators of the human insulin promoter. Chem Biol. 2012; 19:806–818. [PubMed: 22840769]
25. Hertz R, Sheena V, Kalderon B, Berman I, Bar-Tana J. Suppression of hepatocyte nuclear factor-4α by acyl-CoA thioesters of hypolipidemic peroxisome proliferators. Biochem Pharmacol. 2001; 61:1057–1062. [PubMed: 11301038]
26. Blight KJ, Kolykhalov AA, Rice CM. Efficient initiation of HCV RNA replication in cell culture. Science. 2000; 290:1972–1974. [PubMed: 11110665]
27. Tanaka N, et al. PPARα activation is essential for HCV core protein-induced hepatic steatosis and hepatocellular carcinoma in mice. J Clin Invest. 2008; 118:683–694. [PubMed: 18188449]

28. Dharancy S, et al. Impaired expression of the peroxisome proliferator-activated receptor alpha during hepatitis C virus infection. Gastroenterology. 2005; 128:334–342. [PubMed: 15685545]
29. Miyanari Y, et al. The lipid droplet is an important organelle for hepatitis C virus production. Nat Cell Biol. 2007; 9:1089–1097. [PubMed: 17721513]
30. Kapadia SB, Chisari FV. Hepatitis C virus RNA replication is regulated by host geranylgeranylation and fatty acids. Proc Natl Acad Sci USA. 2005; 102:2561–2566. [PubMed: 15699349]
31. Avior Y, et al. Microbial-derived lithocholic acid and vitamin K2 drive the metabolic maturation of pluripotent stem cells-derived and fetal hepatocytes. Hepatology. 2015; 62:265–278. [PubMed: 25808545]
32. Corey KE, et al. Hepatitis C virus infection and its clearance alter circulating lipids: implications for long-term follow-up. Hepatology. 2009; 50:1030–1037. [PubMed: 19787818]
33. Avior Y, Bomze D, Ramon O, Nahmias Y. Flavonoids as dietary regulators of nuclear receptor activity. Food Funct. 2013; 4:831–844. [PubMed: 23598551]
34. Wieland S, et al. Simultaneous detection of hepatitis C virus and interferon stimulated gene expression in infected human liver. Hepatology. 2014; 59:2121–2130. [PubMed: 24122862]
35. Kandathil AJ, et al. Use of laser capture microdissection to map hepatitis C virus-positive hepatocytes in human liver. Gastroenterology. 2013; 145:1404–1413. [PubMed: 23973767]
36. Merquiol E, et al. HCV causes chronic endoplasmic reticulum stress leading to adaptation and interference with the unfolded protein response. PLoS One. 2011; 6:e24660. [PubMed: 21949742]
37. Okuda M, et al. Mitochondrial injury, oxidative stress, and antioxidant gene expression are induced by hepatitis C virus core protein. Gastroenterology. 2002; 122:366–375. [PubMed: 11832451]
38. Liu J, et al. Enhancement of canonical Wnt/β-catenin signaling activity by HCV core protein promotes cell growth of hepatocellular carcinoma cells. PLoS One. 2011; 6:e27496. [PubMed: 22110662]
39. Yamagata K, et al. Mutations in the hepatocyte nuclear factor-4α gene in maturity-onset diabetes of the young (MODY1). Nature. 1996; 384:458–460. [PubMed: 8945471]
40. Qadri I, Iwahashi M, Kullak-Ublick GA, Simon FR. Hepatocyte nuclear factor (HNF) 1 and HNF4 mediate hepatic multidrug resistance protein 2 up-regulation during hepatitis C virus gene expression. Mol Pharmacol. 2006; 70:627–636. [PubMed: 16670373]
41. Matsui C, et al. Hepatitis C virus infection suppresses GLUT2 gene expression via downregulation of hepatocyte nuclear factor 1α. J Virol. 2012; 86:12903–12911. [PubMed: 22993150]
42. Vastag L, Koyuncu E, Grady SL, Shenk TE, Rabinowitz JD. Divergent effects of human cytomegalovirus and herpes simplex virus-1 on cellular metabolism. PLoS Pathog. 2011; 7:e1002124. [PubMed: 21779165]
43. Yamane D, et al. Regulation of the hepatitis C virus RNA replicase by endogenous lipid peroxidation. Nat Med. 2014; 20:927–935. [PubMed: 25064127]
44. Goldwasser J, et al. Naringenin inhibits the assembly and long-term production of infectious hepatitis C virus particles through a PPAR-mediated mechanism. J Hepatol. 2011; 55:963–971. [PubMed: 21354229]
45. Vacca M, et al. Nuclear receptors in regenerating liver and hepatocellular carcinoma. Mol Cell Endocrinol. 2013; 368:108–119. [PubMed: 22789748]
46. Wang C, et al. Identification of FBL2 as a geranylgeranylated cellular protein required for hepatitis C virus RNA replication. Mol Cell. 2005; 18:425–434. [PubMed: 15893726]
47. Nahmias Y, et al. Apolipoprotein B-dependent hepatitis C virus secretion is inhibited by the grapefruit flavonoid naringenin. Hepatology. 2008; 47:1437–1445. [PubMed: 18393287]
48. Teng MW, et al. An endogenous accelerator for viral gene expression confers a fitness advantage. Cell. 2012; 151:1569–1580. [PubMed: 23260143]
49. Folmes CDL, et al. Somatic oxidative bioenergetics transitions into pluripotency-dependent glycolysis to facilitate nuclear reprogramming. Cell Metab. 2011; 14:264–271. [PubMed: 21803296]

50. Fu D, et al. Coordinated elevation of mitochondrial oxidative phosphorylation and autophagy help drive hepatocyte polarization. Proc Natl Acad Sci USA. 2013; 110:7288–7293. [PubMed: 23589864]
51. Clarke B, Wyatt KM, McCormack JG. Ranolazine increases active pyruvate dehydrogenase in perfused normoxic rat hearts: evidence for an indirect mechanism. J Mol Cell Cardiol. 1996; 28:341–350. [PubMed: 8729066]
52. Urizar NL, et al. A natural product that lowers cholesterol as an antagonist ligand for FXR. Science. 2002; 296:1703–1706. [PubMed: 11988537]
53. Izamis M-L, et al. In situ metabolic flux analysis to quantify the liver metabolic response to experimental burn injury. Biotechnol Bioeng. 2011; 108:839–852. [PubMed: 21404258]
54. Nahmias Y, et al. A novel formulation of oxygen-carrying matrix enhances liver-specific function of cultured hepatocytes. FASEB J. 2006; 20:2531–2533. [PubMed: 17077286]
55. Lee K, Berthiaume F, Stephanopoulos GN, Yarmush DM, Yarmush ML. Metabolic flux analysis of postburn hepatic hypermetabolism. Metab Eng. 2000; 2:312–327. [PubMed: 11120643]
56. Chan C, Berthiaume F, Lee K, Yarmush ML. Metabolic flux analysis of hepatocyte function in hormone- and amino acid-supplemented plasma. Metab Eng. 2003; 5:1–15. [PubMed: 12749840]
57. Zhang J, et al. Measuring energy metabolism in cultured cells, including human pluripotent stem cells and differentiated cells. Nat Protoc. 2012; 7:1068–1085. [PubMed: 22576106]
58. Mas VR, et al. Genes involved in viral carcinogenesis and tumor initiation in hepatitis C virus-induced hepatocellular carcinoma. Mol Med. 2009; 15:85–94. [PubMed: 19098997]
59. Huang W, Sherman BT, Lempicki RA. Systematic and integrative analysis of large gene lists using DAVID bioinformatics resources. Nat Protoc. 2009; 4:44–57. [PubMed: 19131956]
60. Miao J, Fang S, Bae Y, Kemper JK. Functional inhibitory cross-talk between constitutive androstane receptor and hepatic nuclear factor-4 in hepatic lipid/glucose metabolism is mediated by competition for binding to the DR1 motif and to the common coactivators, GRIP-1 and PGC-1α. J Biol Chem. 2006; 281:14537–14546. [PubMed: 16492670]

Europe PMC Funders Author Manuscripts

Europe PMC Funders Author Manuscripts

Editorial Summary

AOP: A metabolomics analysis finds that host glycolysis, fatty acid oxidation, the urea cycle, cholesterol biosynthesis and oxidative phosphorylation are modified by hepatitis C virus infection. These effects are mediated through nuclear receptor transcription factors HNF4α, PPARα and FXR.

Europe PMC Funders Author Manuscripts

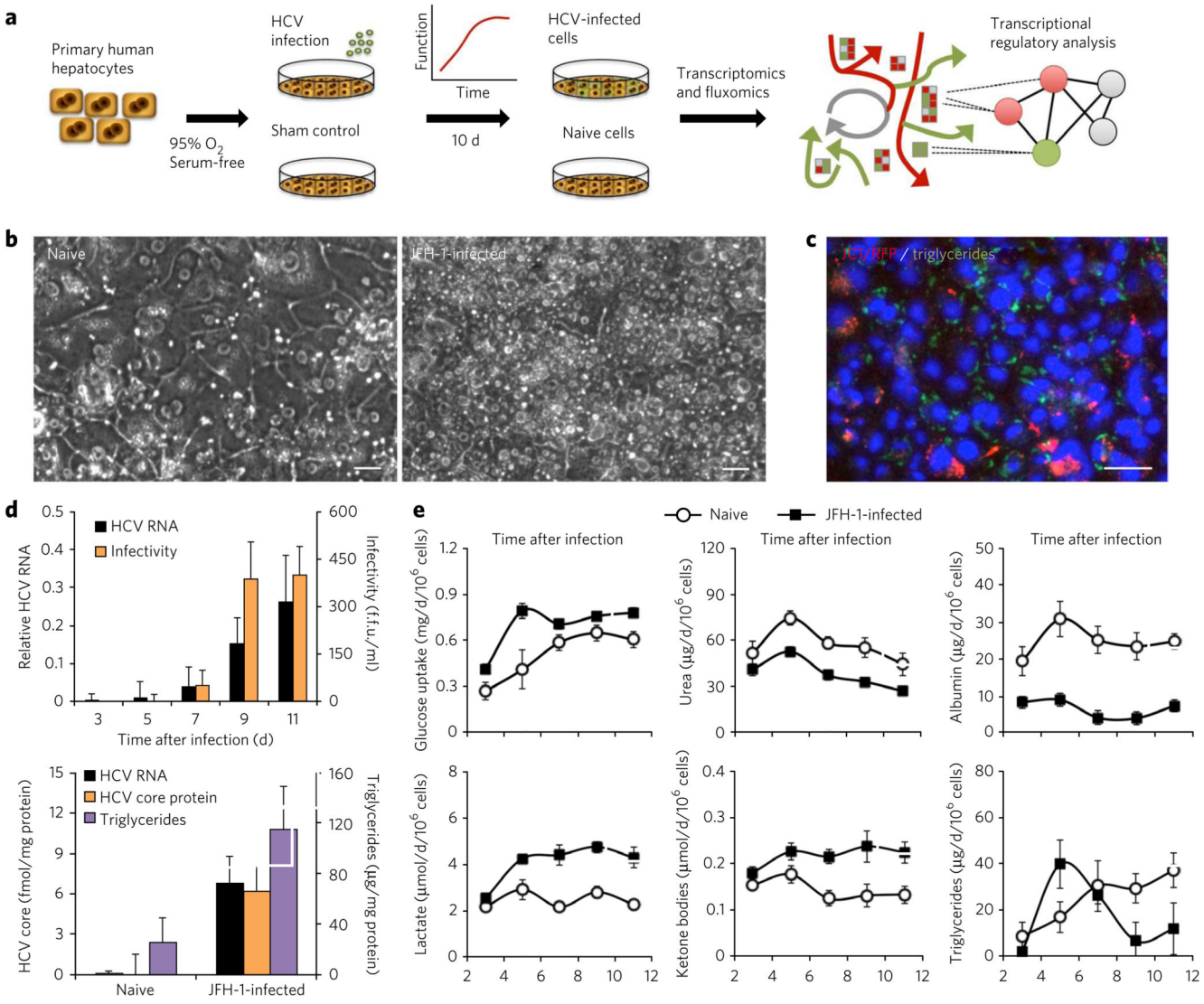

Figure 1. Metabolic fingerprint of HCV infection in oxygenated cocultures of primary human hepatocytes.

(**a**) Schematic of the experimental design. Primary human hepatocytes were cocultured with lung endothelial cells under high-oxygen, serum-free conditions. Cultures were infected with cell culture variants of HCV (JFH-1 or JC1), and their metabolic function was tracked for 10 d in culture. Once metabolism had restabilized, we carried out metabolic flux analysis to identify differentially activated metabolic pathways. Transcriptional regulatory analysis was used to identify the upstream regulators by their differentially activated target genes in each metabolic pathway. (**b**) Phase images of naive and JFH-1-infected cultures on day 10 post-infection. Numerous droplets are seen in infected cells. (**c**) Fluorescent image of JC1-RFP-infected culture counterstained for neutral lipids on day 10 post-infection. (**d**) Top, production of HCV RNA and infectious virus titer as a function of time post-infection, normalized to a culture of Huh7.5.1 infected with JFH-1 ($n = 3$). Bottom, intracellular levels of HCV core protein, HCV RNA and triglycerides on day 10 post-infection ($n = 3$). (**e**)

Changes in glucose uptake and in production of urea, albumin, lactate, ketone bodies and triglycerides in naive and HCV-infected primary hepatocytes. *$P < 0.05$; **$P < 0.001$; n refers to the number of experimental replicates.

Europe PMC Funders Author Manuscripts

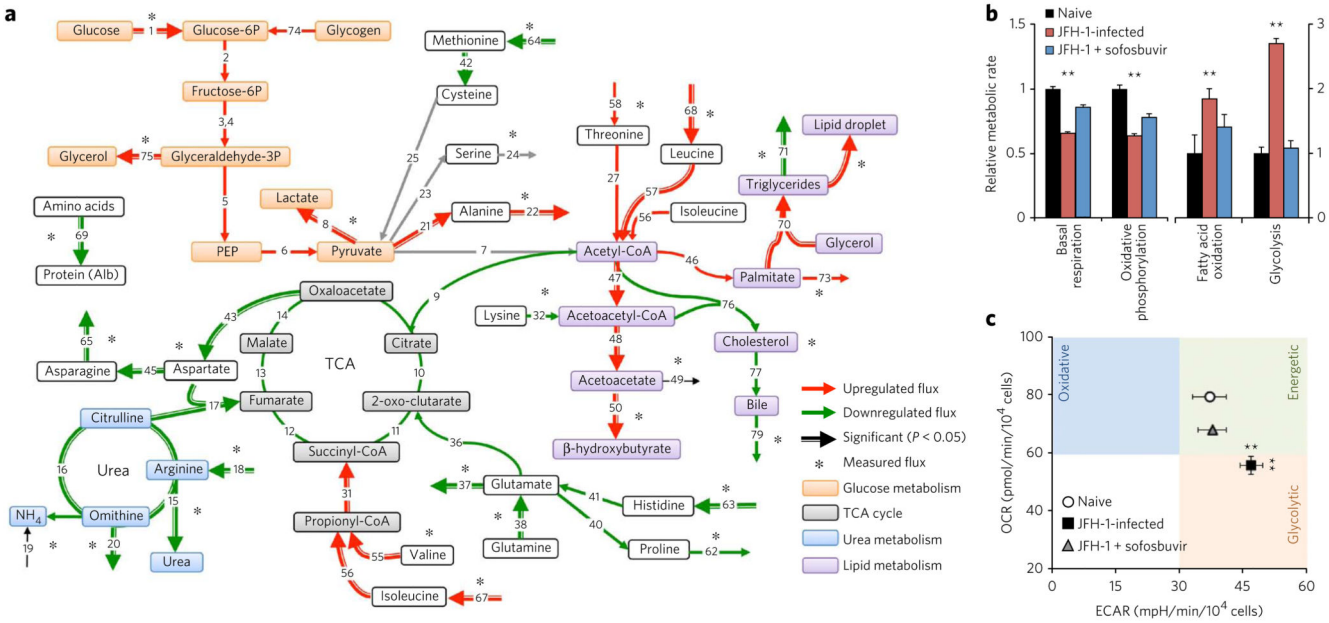

Figure 2. Respiratory and glycolytic flux analysis of HCV-infected and sofosbuvir-treated primary human hepatocytes.

(**a**) Metabolic flux balance map of JFH-1-infected primary hepatocytes compared to naive cells. “Upregulated flux” and “downregulated flux” refer to changes in after infection. Statistically significant changes determined by $P < 0.05$ ($n = 3$). Metabolic fluxes measured by targeted metabolomics or HPLC are marked with an asterisk. TCA, tricarboxylic acid. (**b**) Flux measurements (Supplementary Fig. 2) of mitochondrial basal respiration, oxidative phosphorylation, glycolysis and fatty acid oxidation, normalized to naive cells. JFH-1 infection caused a 34% drop in mitochondrial function and a 36% drop in oxidative phosphorylation ($P < 0.0001$, $n = 3$). Sofosbuvir reversed this effect, but function remained significantly lower in sofosbuvir-treated cells than in naive cells ($P < 0.001$, $n = 3$). JFH-1 infection increased fatty acid oxidation by 85% ($P < 0.02$, $n = 3$) and glycolysis by 169% ($P < 4 \times 10^{-5}$, $n = 3$); both effects were drastically diminished by treatment with sofosbuvir ($P > 0.05$, $n = 3$). (**c**) Metabolic phenotype graph of naive cells, JFH-1-infected cells and infected cells treated with sofosbuvir, showing the metabolic shift toward glycolysis in HCV-infected cells and its reversal after sofosbuvir treatment ($n = 3$). $^{**}P < 0.001$; n refers to experimental replicates.

Europe PMC Funders Author Manuscripts

Europe PMC Funders Author Manuscripts

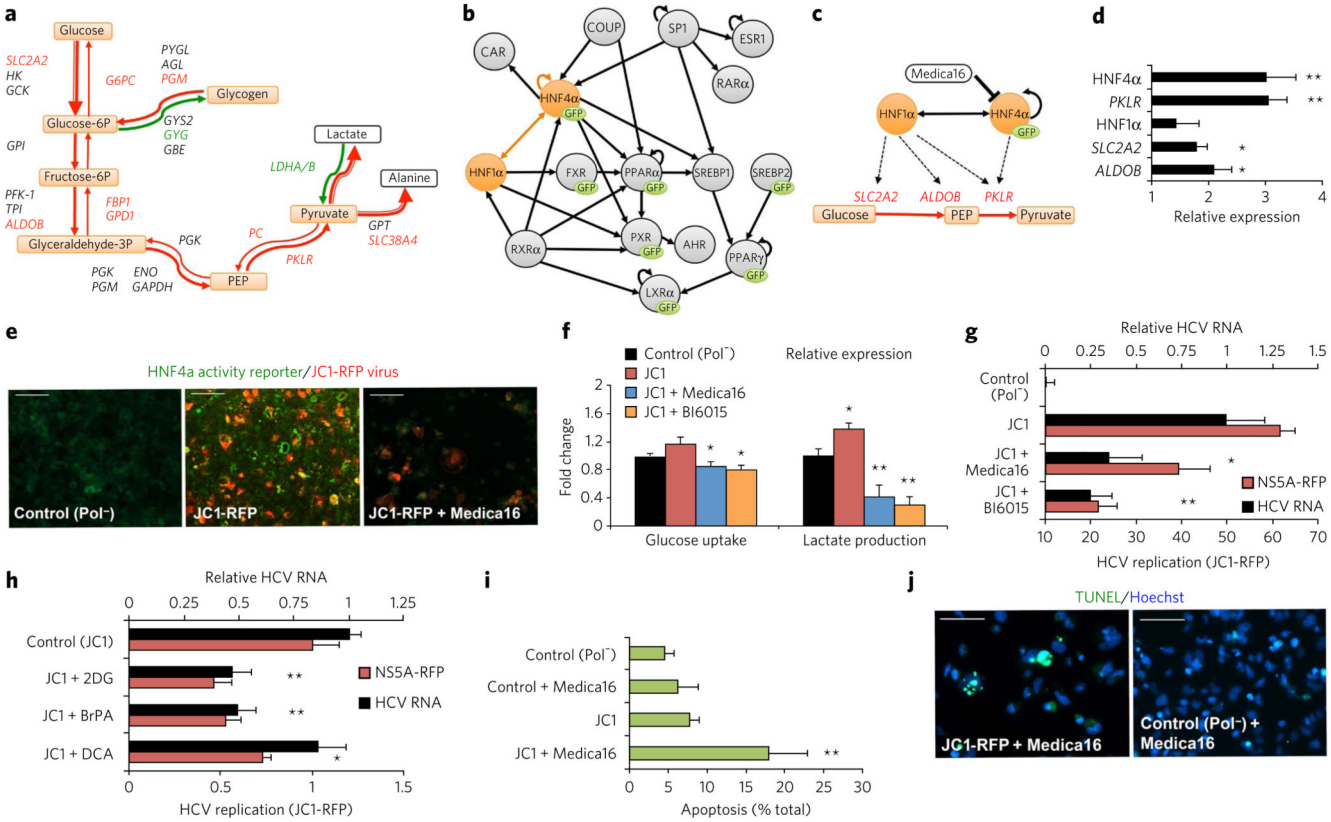

Figure 3. HCV-infected cells become dependent on HNF4α-induced glycolysis.

(**a**) Schematic of hepatic glycolysis showing metabolic fluxes and involved genes. Red, upregulated fluxes and genes; green, downregulated. (**b**) Transcriptional regulatory analysis of glycolysis showed enrichment of HNF4α and HNF1α targets. (**c**) Interaction network of the identified regulators HNF4α and HNF1α, their differentially expressed target genes, and glucose metabolism. (**d**) qRT-PCR showed a threefold increase in expression of HNF4α and its target gene *PKLR* ($P < 0.001$, $n = 3$). Although HNF1α expression did not increase significantly, the expression of its target genes *SLC2A2* and *ALDOB* did significantly increase ($P < 0.05$, $n = 3$). (**e**) HNF4α GFP reporter activity was fourfold greater ($P < 0.001$, $n = 3$) in JC1-RFP-infected Huh7.5.1 cells compared to Pol$^-$ controls. Inhibition of HNF4α with Medica16 blocked its activation[25] while simultaneously decreasing JC1-RFP expression. Scale bars, 10 μm. (**f**) JC1-RFP-infected Huh7.5.1 cells showed increased glucose uptake and lactate production ($P < 0.05$, $n = 5$). Stimulation with HNF4α inhibitors Medica16 and BI6015 reversed the increase in glycolysis ($P < 0.001$, $n = 5$; Supplementary Fig. 6). (**g**) Inhibition of HNF4α with Medica16 ($P = 0.016$, $n = 3$) or BI6015 ($P < 0.001$, $n = 3$) led to decreased expression of both HCV RNA and NS5A-RFP. (**h**) Inhibition of glycolysis with 2DG ($P = 0.004$, $n = 3$) or BrPA ($P = 0.003$, $n = 3$) led to a twofold decrease in HCV replication. (**i**) Cellular apoptosis increased by fourfold in JC1-RFP-infected cells exposed to Medica16 ($P < 0.001$, $n = 3$), whereas Pol$^-$ control cells showed no response. (**j**) Fluorescent micrographs of apoptotic nuclei (green) in Medica16-treated JC1-RFP-infected cells and Pol$^-$ controls. Scale bars, 50 μm. *$P < 0.05$, **$P < 0.001$; n refers to experimental replicates.

Europe PMC Funders Author Manuscripts

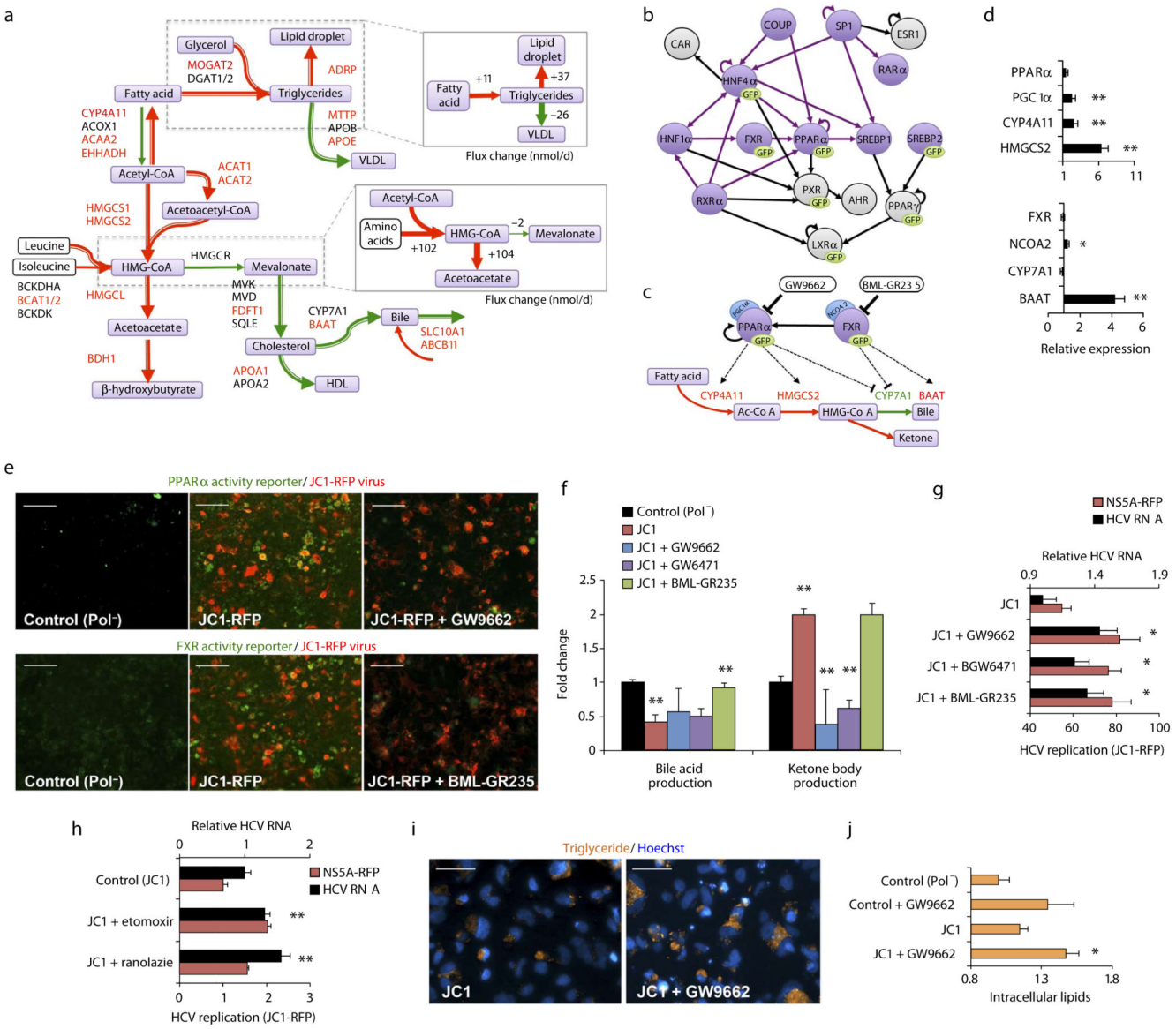

Figure 4. HCV induction of PPARα- and FXR-dependent lipid oxidation is a host antiviral metabolic response.

(**a**) Schematic of fatty acid metabolism, triglyceride synthesis and bile acid production showing metabolic fluxes and involved genes. Red, upregulated fluxes and genes; green, downregulated flux. Panels at right show quantitative changes leading to intracellular lipid accumulation (top) and hypolipidemia (bottom). (**b**) Transcriptional regulatory analysis of lipid metabolism showed significant enrichment of PPARα and FXR, known regulators of fatty acid oxidation and cholesterol biosynthesis. (**c**) Interaction network of PPARα and FXR, their target genes, and lipid metabolism. (**d**) qRT-PCR showed no change in the expression of PPARα and FXR, but their coactivators and target genes were significantly induced. (**e**) PPARα and FXR GFP reporter activity increased by threefold in JC1-RFP-infected Huh7.5.1 cells. Inhibition of PPARα with GW9662 and of FXR with BML-GR235 blocked their activation but increased viral replication. Scale bars, 10 μm. (**f**) JC1-RFP-

infected Huh7.5.1 cells showed a twofold decrease in bile acid production and a twofold increase in ketone body production. BML-GR235 reversed the decrease in bile acid production, and GW9662 and GW6471 reversed the increase in ketone body production. (**g**) Inhibition of PPARα or FXR led to an increase in HCV RNA and NS5A-RFP expression. (**h**) Inhibition of fatty acid oxidation with etomoxir or ranolazine led to an increase in HCV replication. (**i**) Fluorescent micrographs of intracellular lipids (red) in GW9662-treated and untreated cells. Scale bars, 100 μm. (**j**) Intracellular lipid accumulation after PPARα inhibition ($n = 3$). *$P < 0.05$, **$P < 0.001$; n refers to experimental replicates.

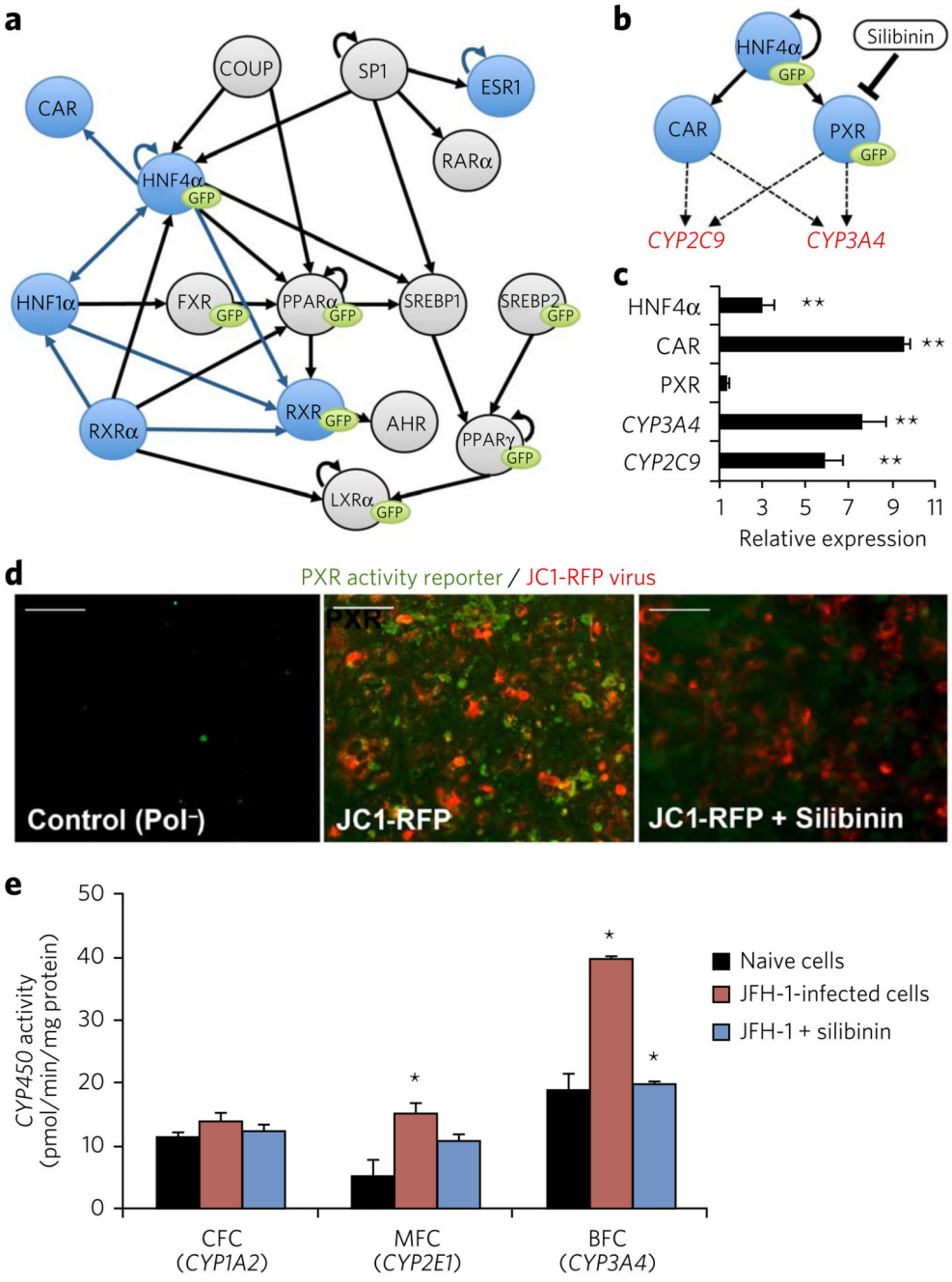

Figure 5. HCV activates PXR and induces CYP450 expression.

(**a**) Transcriptional regulatory analysis of drug metabolism showed significant enrichment in a number of transcription factors, including PXR and CAR, known regulators of CYP450 expression. Inferred regulators of drug metabolism are highlighted in blue on the full regulatory network (Supplementary Table 4). (**b**) Interaction network of the identified regulators HNF4α, PXR and CAR, and their differentially expressed targets. (**c**) qRT-PCR showed no change in the expression of PXR but a ninefold induction of CAR ($P < 0.001$, $n = 3$). PXR and CAR target genes *CYP3A4* and *CYP2C9* were upregulated eightfold and

sixfold, respectively ($P < 0.001$, $n = 3$). (**d**) PXR GFP reporter activity was fivefold greater ($P < 0.05$, $n = 3$) in JC1-RFP-expressing Huh7.5.1 cells compared to Pol^{-} controls. Inhibition of PXR with silibinin blocked its activation without affecting viral replication (Supplementary Fig. 8). Scale bars, 10 μm. (**e**) Functional assays showed a twofold induction of *CYP3A4* activity ($P < 0.005$, $n = 3$) and a threefold induction of *CYP2E1* activity ($P = 0.013$, $n = 3$) in HCV-infected primary hepatocytes. PXR-controlled *CYP3A4* was completely blocked by silibinin. *$P < 0.05$; **$P < 0.001$; n refers to experimental replicates.

Europe PMC Funders Author Manuscripts

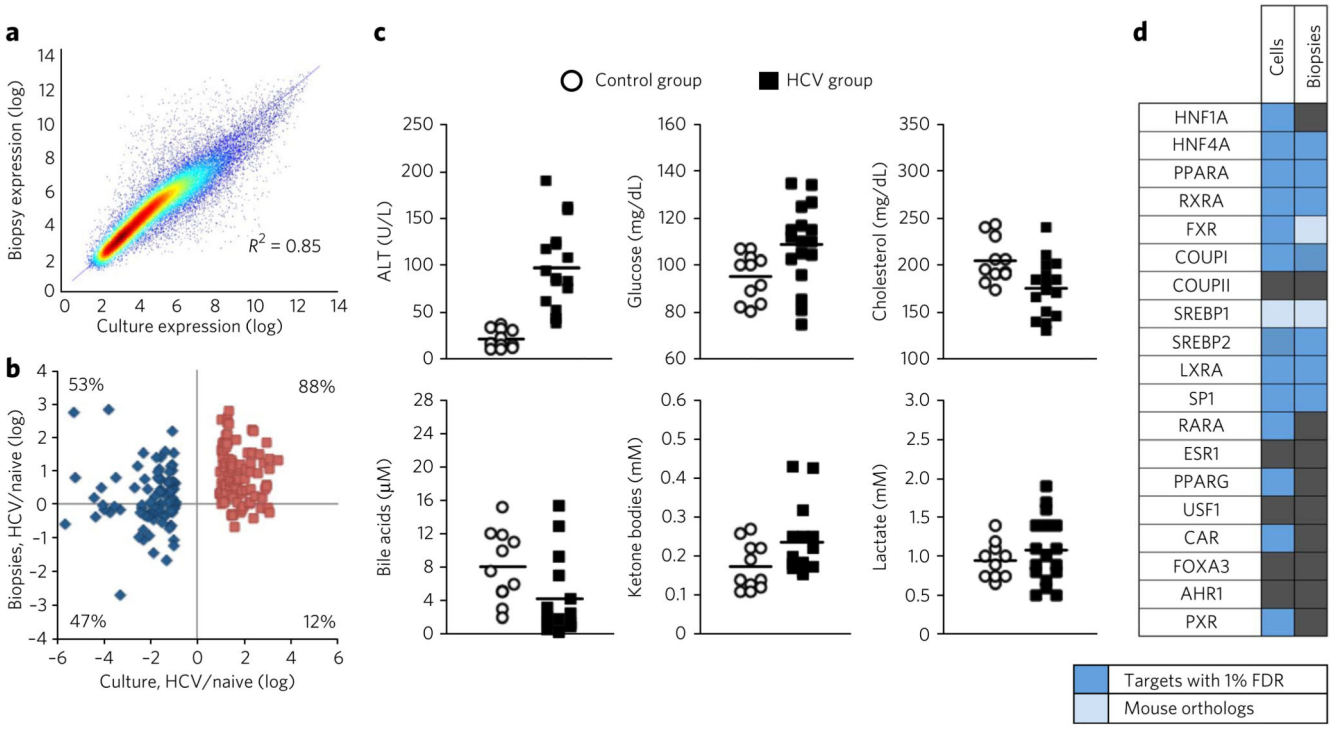

Figure 6. Clinical biopsy and serum samples validate experimental model results.

(**a**) Log-scale scatter plot of whole-genome gene expression correlating *in vitro* expression levels with expression in biopsy samples from healthy liver. R^2 was 0.85, compared with 0.72 for HepG2 cells. (**b**) Log-scale scatter plot of virus-induced gene expression *in vitro* (culture) versus *in vivo* (biopsy). Changes in the expression of genes related to metabolism showed a positive ($P < 0.05$) correlation between *in vivo* and *in vitro* samples. 88% of the metabolic genes upregulated *in vitro* (red squares) were also upregulated *in vivo*, but downregulated genes (blue diamonds) appeared to have randomly distributed *in vivo* expression. (**c**) Metabolic analysis of infected serum samples versus controls. The results confirm previous reports that HCV induces hyperglycemia and hypolipidemia, but they also show a decrease in bile acids and a corresponding increase in ketone bodies and lactate as predicted by the *in vitro* model. (**d**) Unbiased transcriptional regulatory analysis of patient biopsy samples showed activation of key nuclear receptors, mirroring those identified *in vitro*.

Europe PMC Funders Author Manuscripts